Probabilistic Segmentation of Volume Data for Visualization Using SOM-PNN Classifier

Feng Ma[1], Wenping Wang[2], Wai Wan Tsang[2], Zesheng Tang[1], Shaowei Xia[1], Xin Tong[1]

[1]Tsinghua University, P. R. China
[2]The University of HongKong, HongKong

Abstract

We present a new probabilistic classifier, called SOM-PNN classifier, for volume data classification and visualization. The new classifier produces probabilistic classification with Bayesian confidence measure which is highly desirable in volume rendering. Based on the SOM map trained with a large training data set, our SOM-PNN classifier performs the probabilistic classification using the PNN algorithm. This combined use of SOM and PNN overcomes the shortcomings of the parametric methods, the non-parametric methods, and the SOM method. The proposed SOM-PNN classifier has been used to segment the CT sloth data and the 20 human MRI brain volumes resulting in much more informative 3D rendering with more details and less artifacts than other methods. Numerical comparisons demonstrate that the SOM-PNN classifier is a fast, accurate and probabilistic classifier for volume rendering.

CR Categories and Subject Descriptors: I.4.6 [Image Processing and Computer Vision]: Segmentation - Pixel Classification; I.5.1 [Pattern Recognition]: Models - Neural Nets. Additional Keywords: medical image segmentation, multiscale, wavelet transform, SOM, PNN, SOM-PNN classifier, 3D volume rendering

1 INTRODUCTION

Segmentation, or classification, is defined as dividing a data set into components with distinctive characteristics. Many methods have been developed for CT or MR images segmentation, including statistical segmentation [15], model-based methods [7], snake methods [8] and the neural network approaches [6,13].

Feng Ma, Shaowei Xia, Department of Automation, Tsinghua University, Beijing, 100084, P. R. China. Email: swxia@tsinghua.edu.cn.
Wenping Wang, Wai Wan Tsang, Department of Computer Science, The University of HongKong, Pokfulam Road, HongKong. Email: wenping@cs.hku.hk.
Zesheng Tang, Xin Tong, Department of Computer Science, Tsinghua University, Beijing, 100084, P. R. China. Email: ztang@tsinghua.edu.cn.

However, few of these classifiers produce probabilistic classification, which is highly desirable in volume rendering [4].

Traditionally, mixture models are often used for data segmentation in volume rendering [2,4]. In these models, voxels are modeled as compositions of one or more materials. Different material attributes, such as the light intensity and transparency, are determined by the percentages of constituent materials. Thus in this setting probabilistic classifiers are more desirable than all-or-none methods in reducing artifacts in rendering. Classification is given in terms of the percentage of each material from the original data.

For each voxel in the volume data represented by a d dimensional feature vector $x \in R^d$, the percentage of material i in this voxel is determined by the posterior probability

$$p(i|x) = \frac{p(x|i)}{\sum_{k=1}^{K} p(x|k)} \tag{1}$$

where $p(x|k)$ is the class conditional probability density of material k of the voxel x and K is the total number of classes [4].

In practice, there are many ways to estimate the probability density functions, such as parametric methods, non-parametric methods and semi-parametric methods [1]. The parametric approach assumes a specific form of the density function, usually the normal distribution, with a number of parameters to be optimized by fitting the model to the data set. Maximum likelihood (ML) method is usually used to find the optimal values of the parameters. For an image pixel represented by d dimensional feature vector $x \in R^d$, the normally distributed density function is

$$p(x) = \frac{1}{(2\pi)^{d/2}|\chi|^{1/2}} e^{\left\{-\frac{1}{2}(x-\mu)^T \chi^{-1}(x-\mu)\right\}} \tag{2}$$

with parameters $\{\mu, \chi\}$, where μ is the d dimensional mean vector and χ is the $d \times d$ covariance matrix. The parameters are estimated as

$$\bar{\mu} = \frac{1}{N} \sum_{n=1}^{N} x_n \tag{3}$$

$$\bar{\chi} = \frac{1}{N} \sum_{n=1}^{N} (x_n - \bar{\mu})(x_n - \bar{\mu})^T \tag{4}$$

given a data set $X \equiv \{x_1, x_2, \cdots, x_N\}$.

Though ML method is straightforward and easy to implement, the particular form of the density functions chosen might be incapable of providing a precise representation of the true density. In contrast, non-parametric estimation does not assume a particular functional form, but allows the density function to be

determined entirely by the data [14]. Such methods typically suffer from the drawbacks of requiring all the data points to be stored and the slow speed of evaluating a new data point. In the semi-parametric method, a mixture distribution is used to estimate the density function. In the mixture distribution, the density function is again formed from a linear combination of basis functions, whereas the number of basis functions is a parameter of the model itself and can be varied independently from the size of the data set. A general class of functional forms is also allowed as in the non-parametric method. The Expectation-Maximization (EM) method is an example of the semi-parametric method [1]. However, for each class, in addition to estimating a set of parameters iteratively, the number of the basis functions has to be determined in advance. This raises another problem which has to be solved experimentally.

In this paper, we propose a hybrid classifier, the SOM-PNN classifier in which the density function is estimated simply by the combination of the self-organizing map (SOM) [9] and the probabilistic neural network (PNN) [11,12]. The SOM map is trained with a training set first. The PNN algorithm is then carried out based on the SOM map trained. In addition to the general form of density functions achieved, the number of the kernel functions used in PNN is independent of the training set and much fewer than the number of data points. This makes the estimation of the probability density functions much easier and faster.

Feature vectors play an important role in statistical pattern recognition. According to the scale-space theory [5], Gaussian and all its partial derivatives form a complete operator family of an image. We adopt this idea and form our feature vector in the proposed SOM-PNN classifier using the multiscale technique based on the wavelet transform [3], as described by Mallat [10].

We apply our method to sloth CT data and MRI human brain volume data classification. The probabilistically classified volumes are rendered with the direct volume rendering technique [16]. In both cases, higher quality rendered images and better numerical results have been achieved with the SOM-PNN classifier than with other methods.

The remainder of this paper is organized as follows. Section 2 gives the background of multiscale image structure and wavelet transform. Section 3 presents the PNN, SOM algorithms and our new SOM-PNN classifier. Experimentation results and conclusions are given in Sections 4 and 5 respectively.

2 MULTISCALE IMAGE FEATURE VECTOR EXTRACTION USING WAVELET TRANSFORM

It has been shown that the only operator family satisfying the natural front-end vision constraints of linearity, shift variance, rotation variance, and scale invariance is the Gaussian and all its partial derivatives [5]. This operator family provides a complete representation of image structure. For two-dimensional images, the five irreducible invariants of up to second order derivatives can be represented using tensor notations

$$\{L, L_i L_i, L_{ii}, L_i L_{ij} L_j, L_{ij} L_{ji}\} \tag{5}$$

where L is the image intensity, $L_i L_i$ the squared norm of the gradient, and L_{ii} the Laplacian of the image. It has been shown that the segmentation of intensity images can be done using only the zero and first derivatives of the Gaussian, while the second order derivatives are useful when dealing with textured images [6].

The numerical calculation of these elements can be performed with the type of wavelet transform described by Mallat [10] when the Gaussian is used as the smoothing function in the wavelet transform. For each pixel in the image, our feature vector is then formed by 9 components: the original intensity value, the smoothed intensity value and the gradient magnitude of the smoothed images from scale 1 to scale 4 by following this idea. Let

$$\theta_s(x,y) = \frac{1}{s^2}\theta(\frac{x}{s}, \frac{y}{s}) \tag{6}$$

be the dilation of the smoothing function $\theta(x,y)$ at scale s. The two wavelet functions are

$$\psi^1(x,y) = \frac{\partial\theta(x,y)}{\partial x}$$

$$\psi^2(x,y) = \frac{\partial\theta(x,y)}{\partial y} \tag{7}$$

The dilations of the wavelet functions at scale s are

$$\psi_s^1(x,y) = \frac{1}{s^2}\psi^1(\frac{x}{s}, \frac{y}{s})$$

$$\psi_s^2(x,y) = \frac{1}{s^2}\psi^2(\frac{x}{s}, \frac{y}{s}) \tag{8}$$

The wavelet transform of the image, $f(x,y)$, at scale s has two components

$$W_s^1 f(x,y) = f * \psi_s^1(x,y)$$

$$W_s^2 f(x,y) = f * \psi_s^2(x,y) \tag{9}$$

Since

$$\begin{pmatrix} W_s^1 f(x,y) \\ W_s^2 f(x,y) \end{pmatrix} = s \begin{pmatrix} \frac{\partial}{\partial x}(f * \theta_s)(x,y) \\ \frac{\partial}{\partial y}(f * \theta_s)(x,y) \end{pmatrix}$$

$$= s\nabla(f * \theta_s)(x,y), \tag{10}$$

the image gradient magnitude at scale s is

$$M_s f(x,y) = \frac{1}{s}\sqrt{\left|W_s^1 f(x,y)\right|^2 + \left|W_s^2 f(x,y)\right|^2} \tag{11}$$

Hence, for each pixel in the image, its smoothed intensity value and the gradient magnitude of the image smoothed at each scale are obtained directly from the discrete wavelet transform.

3 PNN, SOM ALGORITHMS AND THE NEW SOM-PNN CLASSIFIER

3.1 The PNN Algorithm

The probabilistic neural network, or PNN, is originated from Parzen's probability density estimator [11,12]. For a given data set $X \equiv \{x_1, x_2, \cdots, x_N\}$, the Parzen density function estimator is

$$p(x) = \frac{1}{N\sigma^d}\sum_{n=1}^{N} G\left(\frac{\|x - x_n\|}{\sigma}\right) \tag{12}$$

where $x_n \in R^d$, G is the kernel function and σ the scale factor. The kernel function often takes the Gaussian type

$G(x) = \frac{1}{(2\pi)^{d/2}} e^{-\frac{x^2}{2}}$. Based on the conditional probability

density function estimated using (12), a given sample x will be classified as class i if $p(x|i) > p(x|j)$ for all classes $j \neq i$.

Different values of scale factor σ lead to different classification performances. We follow the ideas in [11,12] to find the optimal σ. First, the performance score of the PNN classifier with a given σ is determined by the cross-validation method. In the process of cross-validation, each training sample is temporally removed from the training set and used as the test sample. The remaining training data is then used in the PNN classifier to classify this test sample. If the sample is correctly classified, the performance score is increased by 1. Repeat this procedure for all the training samples go give the final score. Finally, a one dimensional heuristically search is performed to find the optimal σ with the largest performance score.

3.2 The SOM Algorithm

The standard Kohonen map [9] is a useful tool for clustering, topologically organizing and subspace mapping. In most cases, the topology of the SOM is a two dimensional lattice of neurons, each of which is associated with a reference vector connected to an input. Let $x \in R^d$ be the input data vector and $m_i \in R^d$ be the reference vector of map node i. The input data vector is compared with all the m_i in a metric, such as the Euclidean distance. The node with its reference vector yielding the minimum distance to x is selected as the winner node, signified by subscript c, i.e.,

$$\|x - m_c\| = \min_i \{\|x - m_i\|\}, \quad i = 1,2,\cdots,M \quad (13)$$

where M is the total number of nodes.

During the learning process, the reference vector associated with each node is updated with the same input $x(t)$ in the following way

$$m_i(t+1) = m_i(t) + h_{ci}(t)[x(t) - m_i(t)] \quad (14)$$

where t is the discrete-time coordinate and $h_{ci}(t)$ is the neighborhood kernel. The neighborhood kernel here adopts the Gaussian type

$$h_{ci}(t) = \alpha(t) \cdot \exp\left(-\frac{\|r_c - r_i\|^2}{2\sigma^2(t)}\right) \quad (15)$$

where the width of the kernel $\sigma(t)$ and the learning rate $\alpha(t)$ are monotonically decreasing functions of time, and r_i is the two dimensional coordinates of node i in the lattice.

3.3 The Hybrid SOM-PNN Classifier

The traditional PNN algorithm described above uses all the samples in the training set to estimate the probability density functions and perform classification. In image segmentation, a training set often comprises a large number of samples, and the evaluation of a new sample is very slow for such a large training set. On the other hand, data in the training set is not noise free and if the traditional PNN algorithm is used alone, the classification may be affected by the noise.

We propose a SOM-PNN classifier to overcome the difficulties of the traditional PNN algorithm. In the SOM-PNN classifier, reference vectors from each class of the trained SOM map, instead of the original training samples of a large size, are used to estimate the probability density function. Suppose that the trained SOM map has N_k nodes for material with label k and the corresponding reference vectors are m_i^k, $i = 1, 2, ..., N_k$, the probability density function of material k is then estimated by

$$p(x|k) = \frac{1}{N_k (2\pi)^{d/2} \sigma^d} \sum_{i=1}^{N_k} e^{-\frac{|x - m_i^k|^2}{2\sigma^2}} \quad (16)$$

Having obtained the estimated probability density of each material, the probabilistic classification are obtained using formula (1).

Our hybrid approach as described in this section has the following advantages. First, through the use of SOM, the PNN algorithm is released of the burden of having to process a large size training set. Second, since the trained SOM map serves as a good representative of the training samples, its use makes the PNN classifier more robust in the presence of noise data in the original training set. Furthermore, the probabilistic classification, which is highly desirable for visualization but cannot be obtained with SOM alone, is achieved naturally in PNN. Finally, the combination of SOM and PNN determines the number of basis functions in the model automatically and simplifies the process of probability density estimation, as compared with the EM method [1]. The procedures of our algorithm are shown in Fig. 1.

Step 1: SOM training

training set → [SOM and LVQ training] → SOM map
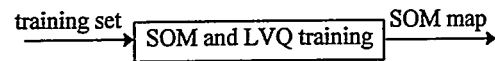
Step 2: PNN classification

SOM map obtained in step 1

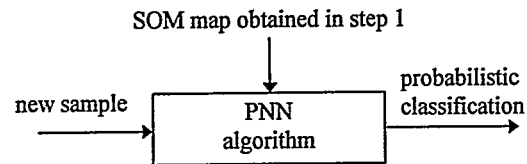new sample → [PNN algorithm] → probabilistic classification

Fig. 1. Diagram of SOM-PNN classifier.

4 EXPERIMENT RESULTS

The proposed SOM-PNN classifier has been built for classifying both CT sloth volume data and MRI human brain volume data. For different kinds of volume data, we apply different strategies in choosing the feature vectors to achieve the best segmentations. Compared to the brain volumes, the CT sloth data is less complicated anatomically. The intensity contrast of image pixels in CT sloth data is also higher than that in MR brain volumes. Moreover, the phenomena of intensity inhomogeneities in CT data are much less apparent than in MR data. To achieve fast and accurate segmentations, for each pixel, we use only the original intensity value and its gradient magnitude at scale 1 to form the feature vector. Adding more components into the feature vector in this case would not improve the performance of the classifier, and would make the algorithm less efficient. However, for the segmentation of more complicated MR brain data to be addressed in the second subsection, we will have to use the complete 9 components feature vector for each pixel as described in Section 2 to get better results.

73

4.1 Sloth CT Volume Classification

The dimensions of the CT sloth data are 128×128×128 with each voxel having 256 gray levels. The task is to segment each voxel in the data set as a composition of four classes: air, fat, soft tissue, and bone.

First, 23643 pixels of different classes were hand-picked from 24 evenly spaced slices in the volume data. According to their intensity levels, these pixels were labeled manually. All these 23643 feature vectors together with their labels form the training set. The SOM with dimensions of 7×11 is set up and trained as described in Section 3.2. By the cross-validation method (see Section 3.1), the optimal scale factor σ is determined to be 0.45. Then the SOM-PNN classifier is applied to each slice of the CT volume.

For comparison, the ML classifier and the PNN algorithm were implemented with the same training set. The SOM map obtained above was also used to classify the CT volume as a separate classifier. Fig. 2 (a) is one original slice image. Its classifications with these four classifiers are shown as Fig. 2 (b) to Fig. 2 (e). In these images, 4 increasing gray levels are assigned to air, fat, soft tissue, and bone pixels. For the probabilistic classifiers, the gray level of a pixel in the classified images is the averaged value of four materials with classified probabilities.
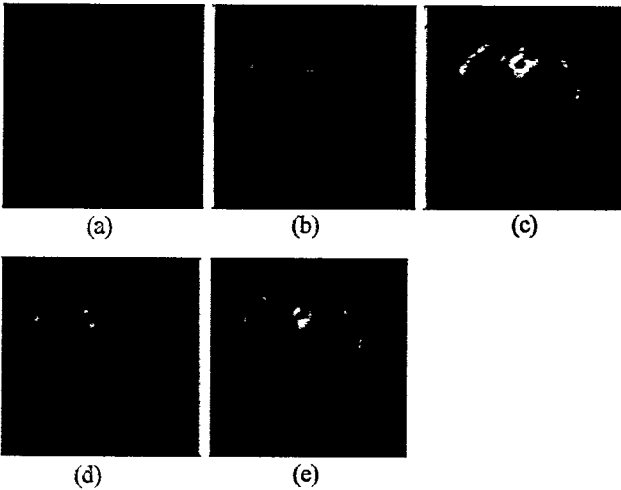

(a)　　　　(b)　　　　(c)

(d)　　　　(e)

Fig. 2. The original slice image (a) and the classifications with the SOM-PNN (b), ML (c), PNN (d) and SOM (e) classifier respectively.

To test the performance of different classifiers, two test sets are selected. Test set 1 consists of 930 soft tissue pixels which are located near to the bone in Fig. 2 (a). Test set 2 consists of 696 bone pixels in the same image without special consideration. The two sets were used to test the classifiers' ability to distinguish the surrounding areas of the bone and the bone itself. For pixel n, let the classified probabilities be $P_n = \{P_{n1}, P_{n2}, \cdots, P_{nK}\}$ and the manually labeled probabilities be $\overline{P_n} = \{\overline{P_{n1}}, \overline{P_{n2}}, \cdots, \overline{P_{nK}}\}$, the correct classification rate of the test set is defined as

$$P_{correct} = 1 - \frac{e}{N}, \qquad (17)$$

where $e = \sum_{n=1}^{N} \sum_{j=1}^{K} \left(P_{nj} - \overline{P_{nj}}\right)^2 \Big/ 2 \qquad (18)$

where K is the number of materials to be classified and N the number of voxels in the test set. Table 1 lists the results.

Table 1 Correct rate of the data sets with different classifiers

	SOM-PNN	ML	PNN	SOM
training set	97.97	97.89	97.85	98.52
test set 1	83.99	66.44	78.56	83.65
test set 2	74.17	74.81	73.36	55.17

Comparing Fig. 2 (c) with Fig. 2 (a), we might conclude that the ML method over-segmented the bone pixels in the image. This agrees with the low correct rate of test set 1 and high correct rate of test set 2 with the ML method in Table 1. It can also been seen from Fig. 2 (e) that bone pixels with low intensity level are not correctly classified with the SOM classifier which accords with the very low correct rate of test set 2 with the SOM classifier. For the three data sets, the SOM-PNN classifier outperforms the PNN classifier due to the clustering ability of SOM.

All the 128 slice images are classified by the above classifiers. The classified images are stacked together to yield a 3D probabilistic classification. On an SGI Indigo2 Maximum IMPACT workstation with 195Mhz R10000 CPU and 192Mb memory, the time used to perform the classification of the whole 3D CT sloth data using the SOM-PNN, ML, PNN and SOM classifiers are 241s, 178s, 48524s and 159s, respectively. The SOM-PNN classifier is about 200 times faster than the PNN classifier. The significant improvement in efficiency makes the proposed SOM-PNN classifier a favorable choice in time-critical applications, where non-parametric methods would be too slow to be used. Moreover, the time that PNN classifier takes varies with different training sets, while the time used by the SOM-PNN classifier is almost the same. The training time of the SOM used in the SOM-PNN classifier is 734s while that of the PNN with the full training set is more than 20 hours on the same machine.

A direct volume rendering method based on 3D texture mapping [16] is used to render the classified data. The rendered images of the volumes classified with the SOM-PNN, ML, PNN and SOM classifiers are shown in Fig. 3, 4, 5 and 6, respectively. In Fig. 4, the front cartilage of the sloth chest is clear and the back ribs are shown to be connected to the spine. But the quality of the image is severely affected by the bone noise. In contrast, the SOM-PNN classifier achieves similar classification of the bone with much less noise as shown in Fig. 3. In Fig. 5, where PNN alone is used, the image quality is also badly affected by the noise due to the noise sample in the training set. Finally, in Fig. 6, the front cartilage disappears entirely and the back ribs are shown to be disconnected to the spine with the SOM classifier.

The above results show that the proposed SOM-PNN classifier works very well in the CT sloth data classification. Numerically it produces nearly the highest overall correct rate for different test sets. The efficiency improvement is also significant. From visual inspections, the SOM-PNN classifier segments the volume data with least noise. Compared to the SOM classifier used in the literature, the segmentation produced using the SOM-PNN classifier reveals anatomically more meaningful structures.

4.2 Human Brain Classification

We also applied the SOM-PNN classifier to human brain data segmentation. The brain volumes are the 20 normal brain volume data sets provided by the Internet Brain Segmentation Repository (IBSR)[1] [17]. The dimensions of these coronal three-dimensional T1-weighted spoiled gradient echo MRI data range from 256x256x51 to 256x256x61. All the volumes have been positionally normalized by imposing a standard three-dimensional brain coordinate system. Manual segmentation is also available from the same source [17], which is obtained with semi-automated segmentation algorithms.

These brain volumes are to be segmented into three classes: Cerebral Spinal Fluid (CSF), gray matter (GM) and white matter (WM). For case 112_2, to apply our method, 16763 brain pixels of these three classes from slice 35 and slice 36 of the volume are selected as the training set. To precisely segment the complicated brain structures in the low intensity contrast images, multiscale feature vectors with the complete 9 components described in Section 2 are extracted using the wavelet transform. The SOM map with dimensions of 13x11 is then established and trained as described in Section 4.1. The correct rate of the training set is 90.87%. The optimal scale factor σ found using the cross-validation method is 0.13. Then the SOM-PNN classifier is applied to each scan of the whole data set to yield a 3D segmentation. A threshold value of 20 is set to separate air pixels from brain pixels. Each pixel with the intensity value greater than 20 is classified into the probabilistic composition of CSF, gray matter and white matter with the SOM-PNN classifier. As in Section 4.1, the ML, PNN and SOM classifiers were implemented with the selected training set and used to segment the same volume. In each segmentation, no post-processing is performed. Fig. 7 (a) is an original brain scan (slice 21), Fig. 7 (b) is the manual segmentation. The segmentations using the SOM-PNN, ML, PNN and SOM classifiers of the same brain scan are presented as Fig. 7 (c) to Fig. 7 (f). The gray levels of air, CSF, gray matter and white matter are assigned in an increasing order. As before, the color of each final pixel is the average of the 3 classes' colors weighted with the classified percentages.

From Fig. 7, it can be seen that the SOM-PNN classifier achieves better segmentation compared to the manual segmentation. As shown in Fig. 7 (e), the PNN algorithm using the original training set results a segmentation similar to the one obtained with the SOM-PNN classifier. In Fig. 7 (d), the ML classifier produces good segmentation in the upper part of the brain but CSF artifacts are produced in the bottom boundary of the brain. Moreover, due to the existence of intra-scan inhomogeneities of the brain pixel intensity, the white matter in the lower part of the brain is under-segmented compared with the SOM-PNN classified segmentation. As seen in Fig. 7 (f), the white matter in the lower part of the brain is largely lost due to non-probabilistic characteristic of the SOM classifier. Although the problems with inter- and intra-scan inhomogeneities are not dealt with in this paper, the proposed SOM-PNN classifier yields reasonable segmentation despite these artifacts.

Classified slices are stacked together to yield a 3D

---

[1] The 20 normal MR brain data sets and their manual segmentations were provided by the Center for Morphometric Analysis at Massachusetts General Hospital and are available at http://neuro-www.mgh.harvard.edu/cma/ibsr.

segmentation. The time used to segment this volume with the SOM-PNN, SOM, ML and PNN classifier is 158s, 134s, 63s and 14470s respectively. Again significant improvement of efficiency is achieved with the SOM-PNN classifier compared with the original PNN algorithm. The classified volumes are rendered with texture mapping hardware. In Fig. 8, the five rendered volumes are clipped coronally with the same viewpoint and clipping depth. In these images, the colors assigned to gray matter, white matter and CSF are red, white and green respectively. From visual inspection, the SOM-PNN classifier, the PNN classifier and the ML classifier yield similar segmentations of gray matter and white matter in the upper part of the brain. The ML classifier over-segments the CSF which leads to the noise in the boundary area of the brain. In the lower part of the brain, due to the existence of intensity inhomogeneities, most of the white matter is lost in the SOM segmentation. For the other 3 methods, i.e., the ML, PNN, and SOM-PNN, the segmentations obtained with the SOM-PNN classifier are closest to the manual segmentation.

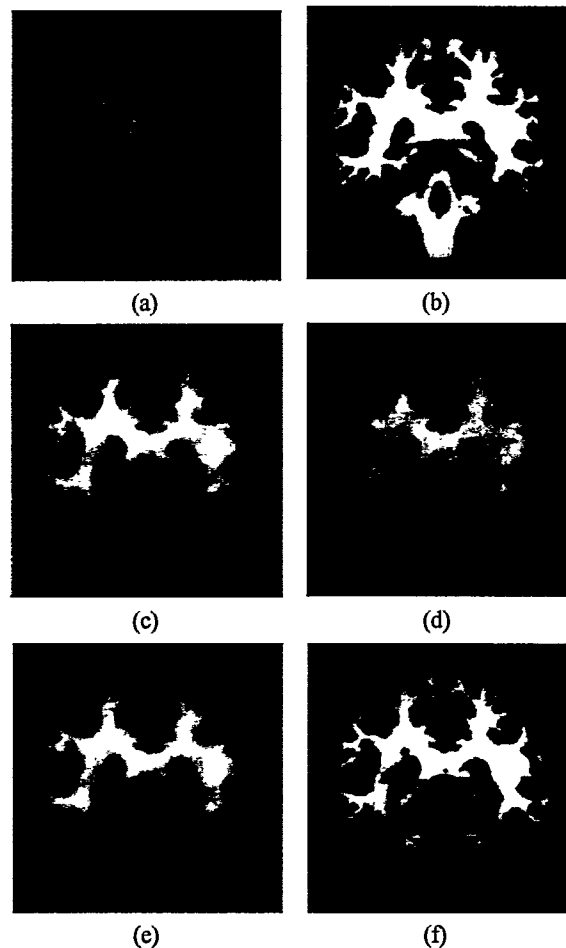(a)   (b)

(c)   (d)

(e)   (f)

Fig. 7. The original brain scan (a), its manual segmentation (b), the segmentations with the SOM-PNN (c), ML (d), PNN (e) and SOM (f) classifier respectively.

For different segmentations, in addition to the visual inspection, numerical metrics are needed to compare them quantitatively. In the literature, there are two metrics often used to compare the similarity between segmentations. One is the overlap metric [17] and the other is the percentage of difference [15]. For a given

voxel class assignment, the overlap metric between two segmentations is defined as the number of voxels that have this class assignment in both segmentations divided by the number of voxels where either of the two segmentations has this class assignment [17]. This metric approaches 1.0 for results that are very similar and is near 0.0 when they share no similarly classified voxels. The percentage of difference between two segmentations is defined as the ratio between the number of differently labeled pixels within the region of interest (ROI) and the total number of pixels within the ROI [15]. The percentage of difference measures the similarity between two segmentations in the ROI globally while the overlap measures each classes separately. Although these two metrics yield a reasonable comparison between two segmentations, they are not appropriate for comparing probabilistic segmentations because pixel counting does not accommodate probabilities associated with probabilistically classified voxels. However, since in the literature, many segmentations are only compared with manual segmentation, in particular the overlap metric in the case of the 20 MR brain volumes, we will also use this metric to compare our results.

To evaluate a probabilistic segmentation with the overlap metric, the probabilistic results must first be converted into non-probabilistic ones. To this end, probabilistically classified voxels are labeled as the class with the largest probability. As with the case 112_2, the other 19 MR brain volumes are classified and tested in the same way. The overlap values of CSF, gray matter and white matter are averaged over these 20 normal cases. Table 2 is the results and the comparison with other methods reported in IBSR [17]. The gray matter overlap metric of different methods for the 20 MR brain volumes is shown in Fig. 9. In Fig. 9, the sequence of the 20 brain volumes is roughly arranged by their difficulty to be segmented. Some volumes that were acquired recently with more sophisticated MR machines have better data qualities and are listed at the end of the sequence.

Table 2 Averaged overlap of 20 normal brain volumes between automatic segmentations and the manual segmentation

methods	CSF	GM	WM
adaptive MAP*	0.069	0.564	0.567
biased MAP*	0.071	0.558	0.562
fuzzy c-means	0.048	0.473	0.567
MAP*	0.071	0.550	0.554
maximum-likelihood	0.062	0.535	0.551
tree-structure k-means	0.049	0.477	0.571
SOM	0.419	0.790	0.682
SOM-PNN	0.389	0.742	0.673
ML	0.130	0.605	0.658
manual**	N/A	0.876	0.832

*MAP means Maximum Aposteriori Probability
** 4 brains averaged over 2 experts

From Table 2 and Fig. 9, it can be seen that the SOM and SOM-PNN classifiers achieve higher overlap with the manual segmentation than the other seven methods. For gray matter, the SOM and SOM-PNN classifier are at least 13% higher than other methods. The most significant improvement is the CSF segmentation. The CSF overlap of all methods in IBSR, with

respect to the manual segmentation, is below 0.1. The CSF overlap of our implementation of ML is only 0.13. However, the CSF overlap of the SOM-PNN classifier with manual segmentation and that of the SOM classifiers have achieved 0.389 and 0.419 respectively. Besides, as seen in Fig. 9, the performance of the SOM and SOM-PNN classifier varies much less significantly than other methods, thus consistent classification has been achieved for these 20 normal MR brain volumes. It is not surprising that the SOM classifier yields better numerical results than the SOM-PNN classifier with the overlap metric because truncation on the probabilistic classification offsets the accuracy of the SOM-PNN classifier.

Since there is a considerable loss of classified information when converting probabilistic segmentation into a non-probabilistic segmentation, to get a more reasonable comparison between the SOM-PNN classifier and the SOM classifier, we now propose a generalized difference ratio metric. For pixel n, let the probabilities of segmentation A be $P_n^A = \{P_{n1}^A, P_{n2}^A, \cdots, P_{nK}^A\}$ and that of segmentation B be $P_n^B = \{P_{n1}^B, P_{n2}^B, \cdots, P_{nK}^B\}$, the generalized difference ratio between A and B is defined as

$$r_{AB} = \frac{1}{N}\sum_{n=1}^{N}\sum_{j=1}^{K}\frac{\left(P_{nj}^A - P_{nj}^B\right)^2}{2} \times 100\% \qquad (19)$$

where N is the total number of voxels in the ROI and K is the number of materials to be segmented. Here the ROI is the brain volume without air and $K = 3$. In the non-probabilistic case, the generalized difference ratio is reduced to the percentage of difference between two segmentation used in [15].

The difference ratios of automatic segmentations and the manual segmentation for the 20 normal brain volumes are listed in Table 3. Three automatic segmentations, SOM-PNN, SOM, and ML, are compared altogether.

Table 3 Difference ratio of the 20 normal brain volumes between automatic segmentation and manual segmentation (%)

brain case	SOM-PNN	SOM	ML
5_8	21.55	22.69	19.63
4_8	18.54	19.85	23.46
2_4	19.01	19.68	29.67
6_10	16.39	21.75	29.49
15_3	17.94	19.62	21.98
16_3	14.98	16.22	21.50
17_3	13.91	16.25	19.36
8_4	13.46	15.54	19.44
7_8	13.82	14.52	22.23
110_3	10.59	12.77	15.83
111_2	11.78	13.56	18.73
112_2	10.52	12.22	15.89
100_23	10.62	11.34	16.88
202_3	9.84	11.04	11.79
191_3	9.62	12.27	15.74
12_3	8.81	9.74	14.07
13_3	9.08	10.97	14.18
1_24	10.41	13.15	17.58
205_3	9.63	10.00	13.89
11_3	10.02	10.82	15.03
average	13.03	14.70	18.82

From Table 3, it can be seen that the averaged difference ratio of the SOM-PNN classifier is 1.67% lower than that of the SOM classifier. Compared with ML method, the SOM-PNN classifier has a 5.8% lower difference ratio. Moreover, this result is quite promising because in [15], the averaged difference ratio is about 20%, though different data sets are used.

The experiment results in this subsection reveal the superiority of the SOM-PNN classifier to other automatic classifiers mentioned above. From 2D and 3D inspection, it produces the closest images to the manual segmentation. Numerically, the SOM-PNN classifier produces much better results than the traditional statistical classifiers with the overlap metric. According to the generalized difference ratio metric, it is also better than the SOM classifier. Compared with the traditional PNN algorithm, the SOM-PNN classifier achieves significant improvement in efficiency and the classification accuracy is also improved.

5 CONCLUSIONS

We have proposed a new probabilistic classifier, the SOM-PNN classifier, for medical data classification and volume rendering. The new classifier is a semi-parametric density estimator and produces probabilistic classification with the Bayesian confidence measure. The volumes segmented using the SOM-PNN classifier reveal anatomically more meaningful structures than non-probabilistic segmentation. Numerically, the SOM-PNN classifier is more accurate than other automatic segmentation methods in both the sloth and the brain cases. The SOM-PNN classifier is also a fast classifier. Based on the noise-free representative reference vectors provided by SOM, the SOM-PNN classifier segments the sloth CT data 200 times faster than the original PNN algorithm.

Essentially, the SOM-PNN classifier is an intensity based classifier and will lose its power when the inter- and intra-scan intensity inhomogeneities present severe problems. However, with the modern MR scanners, this problem has been minimized as indicated by the low difference ratios for the last several cases in the 20 normal brain data sets. In another aspect, the SOM-PNN classifier needs the semi-automatic segmentation of several brain scans and the pre-training of the SOM map as preprocessing steps. By our experience, segmentation of 2 or 3 scans does not present as a big burden, and the pre-training of the SOM in the SOM-PNN classifier can be done in a matter of minutes.

The problem of quantitatively evaluating probabilistically segmentation is raised in this paper. The metrics currently used in literature are suitable for non-probabilistic segmentation and are not appropriate for evaluating the quality of segmentation for volume rendering. For example, although the SOM classifier also produces high overlaps with manual segmentation, the volumes segmented with the SOM classifier lose more details than probabilistically segmented volumes. In this paper, a generalized difference ratio is proposed in order to conduct reasonable comparison among probabilistic classifiers without sacrificing the probabilistic property.

Acknowledgment

References

[1] Christopher M. Bishop, Neural Networks for Pattern Recognition, 1995, Clarendon Press, Oxford, ISBN 0-19-853849-9.

[2] Wenli Cai, et. al., Rendering of Surface and Volume Details in Volume Data, *EUROGRAPHICS'95*, vol. 14, No. 3, 1995, pp. 421-430.

[3] Ingrid Daubechies, Ten Lectures on Wavelets, Philadelphia, Pa.: Society for Industrial and Applied Mathematics, 1992.

[4] Robert A. Drebin, Loren Carpenter, Pat Hanrahan, Volume Rendering, *Computer Graphics*, vol. 22, no. 4, august 1988, pp. 65-74.

[5] L. M. J. Florack, B. M. ter Haar Romeny, J. J. Koenderink, and M. 'A. Viergever, Scale and the Differential Structure of Images, *Image and Vision Computing*, 10(6), July/Aug., 1992, pp. 376-388.

[6] S. Haring, M. A. Viergever, J. N. Kok, A Multiscale Approach to Image Segmentation Using Kohonen Networks, In A. Gmitro and H. H. Barrett, editors, *IPMI, Proc. of the 13th conference*, Springer-Verlag, Berlin, 1993, pp. 212-224.

[7] M. Kamber, D. L. Collins, G. S. Francis, A. C. Evans, Model-Based 3-D Segmentation of Multiple Sclerosis Lesions in Magnetic Resonance Brain Images, *IEEE Trans. on Medical Imaging*, vol. 14, no. 3, Sept. 1995, pp. 442-453.

[8] M. Kass, A. Witkin, D. Terzopoulos, Snakes: Active Contour Models, *Int. J. Comput. Vision.*, vol. 1, 1987, pp. 321-331.

[9] T. Kohonen, The Self-Organizing Map, *Proceedings of the IEEE*, vol. 78, no. 9, 1990, pp. 1464-1480.

[10] S. G. Mallat, and S. Zhong, Characterization of Signals from Multi-scale Edges, *IEEE Trans. Pattern Analysis and machine Intell.*, vol. 14, 1992, pp. 710-723.

[11] Timothy Masters, Practical Neural Network Recipes in C++, Academic Press, San Diego, 1993. ISBN 0-12-479040-2.

[12] Timothy Masters, Advanced Algorithms for Neural Networks: A C++ sourcebook, John Wiley & Sons Inc., New York, 1995. ISBN 0-471-10588-0.

[13] M. Ozkan, B. M. Dawant, and R. J. Maciunas, Neural-Network-Based Segmentation of Multi-Modal Medical Images: A comparative and Prospective Study, *IEEE Trans. on Medical Imaging*, vol. 12, no. 3, Sept. 1993, pp. 534-544.

[14] Ronald H. Randles, Douglas A. Wolfe, Introduction to the Theory of Nonparametric Statistics, New York: Wiley, c1979. ISBN 0-471-04245-5.

[15] W. M. Wells, W. E. L. Grimson, R. Kikinis, and F. A. Jolesz, Adaptive Segmentation of MRI Data, *IEEE Trans. on Medical Imaging*, vol. 15, no. 4, Aug. 1996, pp. 429-442.

[16] Orion Wilson, Allen Van Gelder, Jane Wilhelms, Direct Volume Rendering via 3D Textures, University of California Technical Report, UCSC_CRL_94_19, 1994.
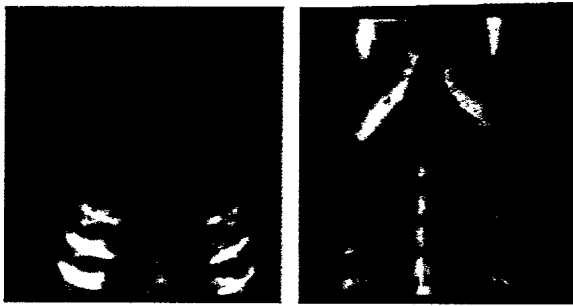
[17] http://neuro-www.mgh.harvard.edu/cma/ibsr.htm.

Fig. 3. Rendered images of the sloth CT volume with SOM-PNN segmentation.

Fig. 4. Rendered images of the sloth CT volume with ML segmentation.

Fig. 5. Rendered images of the sloth CT volume with PNN segmentation.

Fig. 6. Rendered images of the sloth CT volume with SOM segmentation.

Fig. 8. Coronally clipped views of the MRI brain case 112_2 with manual segmentation, SOM-PNN, ML, PNN and SOM segmentations respectively.
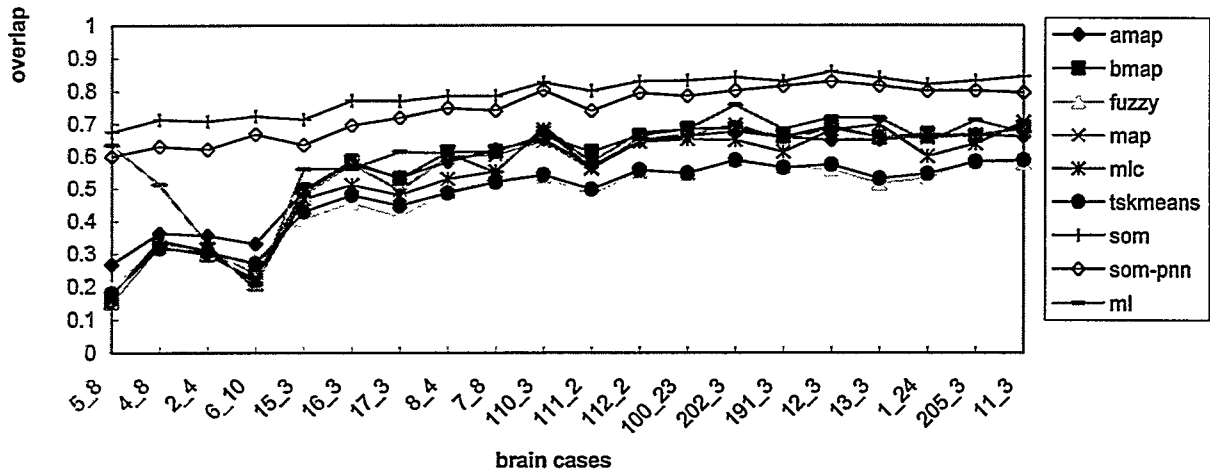

Fig. 9 Gray matter overlap between automatic methods with manual segmentation for the 20 normal MR brain volumes